*bioresources*.com

# Preparation of Highly Porous Binderless Active Carbon Monoliths from Waste Aspen Sawdust

Dawei Li,[a,b] Ruiyuan Tang,[a] Yuanyu Tian,[a,b,*] Yingyun Qiao,[b] and Junhua Li [a]

Waste aspen sawdust was used as a precursor to prepare binderless active carbon monoliths (ACMs) with high porosities. The ACMs were prepared by activation with $H_3PO_4$ at different activation temperatures (500 to 700 °C) and retention times (1 to 3 h). Their morphologies, yields, textural properties, and microcrystalline structures were investigated using scanning electron microscopy (SEM), an analytical balance, $N_2$ adsorption/desorption techniques, and X-ray diffraction (XRD). The results indicated that waste aspen sawdust could be successfully converted into highly porous binderless ACMs. The apparent specific surface area (SSA) and yield of ACMs were in the range of 688 to 951 $m^2$/g and 26.6 to 36.2%, respectively. Highly microporous ACMs with a micropore percentage of 91.1%, apparent specific surface area of 951 $m^2$/g, pore volume of 0.481 mL/g, and bulk density of 0.56 g/mL could be produced by activation at 700 °C for 1 h. Increasing the activation temperature or retention time increased the specific surface area, pore volume, and turbostratic degree, but decreased the yield.

## INTRODUCTION

Active carbon monoliths (ACMs) can be used in gas adsorption, wastewater treatment, catalyst support, and energy storage, because of characteristics such as high mechanical strength, large volumetric adsorption capacity, and ease of transport (Vargas *et al.* 2010; Vargas *et al.* 2012). Hence, they have attracted worldwide attention. ACMs are commonly prepared by the nanocasting strategy, which involves impregnation of a porous ceramic with a carbonaceous solution, or by full-body extrusion, which requires compaction of a mixture of carbon precursors and binders in a mould (Liu *et al.* 2007). However, ACMs can also be produced without using binders through the activation of biomass with $H_3PO_4$ or $ZnCl_2$. So far, binderless ACMs have been prepared from limited types of biomass, including coconut shell (Vargas *et al.* 2009; Vargas *et al.* 2011), African palm cuesco (Vargas *et al.* 2009; Vargas *et al.* 2011), *Pinus sylvestris* (Laszlo *et al.* 2005), olive stone (Nakagawa *et al.* 2007; Djeridi *et al.* 2013), rubber wood sawdust (Taer *et al.* 2011), and hemp cane (Rosas *et al.* 2008).

Korean aspen (*Populus davidiana*) is a fast growing plant widely distributed in northern China, Korea, and Siberia (Si *et al.* 2009). In China, the planting area is close to 20 $Gm^2$. *Populus davidiana* can be processed to produce plywood, fireboards, beams, and packing cases, among others. During the processing of this biomass, plenty of waste

aspen sawdust is yielded, which poses problems like environmental pollution, fire hazards, and space consumption. Conversion of the waste aspen sawdust into ACMs can solve these problems while creating additional value. However, to the best of our knowledge, the use of waste aspen sawdust as a precursor for the production of binderless ACMs has not been studied. This research aimed to convert waste aspen sawdust into binderless ACMs with high porosities. The ACMs were prepared by activation with $H_3PO_4$ at different activation temperatures and retention times. The morphologies, textural properties, microcrystalline structures, and yields were investigated. The obtained ACMs displayed large specific surface areas and might be useful in gas adsorption and wastewater treatment.

## EXPERIMENTAL

### Materials

Waste aspen sawdust was provided by China Qingdao Jiaonanlongquan Wood Processing Co. Ltd. The moisture, ash, volatile matter, and fixed carbon contents, as well as particle size, were 5.3%, 5.0%, 74.1%, 15.7%, and 0.28 to 1.18 mm, respectively, for the used sawdust. $H_3PO_4$ (AR) was bought from Yantai Shuangshuang Co. Ltd. The water used was self-prepared distilled water.

### Preparation of Active Carbon Monoliths

The sieved sawdust (20.0 g) was dried at 110 °C for 2.5 h and then cooled to room temperature in a desiccator. The cooled sawdust (5.0 g) was then impregnated with a 55wt% $H_3PO_4$ solution at a 1:1 sawdust/$H_3PO_4$ mass ratio in a beaker at 85 °C for 2.5 h. The impregnation ratio was fixed at 1:1, because preliminary experiments showed that this ratio allowed production of highly porous ACMs using a small amount of $H_3PO_4$. The beaker was covered with a pore-containing cling film. Subsequently, the cling film was removed to dry the mixture at 85 °C for 2.5 h. In the impregnation and drying steps, the mixture was manually stirred intermittently. The dried mixture (*ca.* 2 g) was pressed in a 2.0-cm inner-diameter cylindrical mould at 20 MPa for 1 min to yield a coin-like monolith. The monolith was then heated under $N_2$ to 500 to 700 °C with a retention time of 1 to 3 h at an average heating rate of 15 °C/min. Afterwards, the carbon monolith was cooled to room temperature under $N_2$ and repeatedly washed with hot distilled water until the eluate pH was neutral. Finally, the washed carbon monolith was dried at 90 °C for 9 h and cooled in a desiccator. During preparation, only two process parameters (activation temperature and retention time) were varied, with the others kept as aforementioned. Hence, the as-prepared active carbon monoliths were recorded as Mx-y, where x and y meant activation temperature and retention time, respectively. For instance, M500-2 represents an active carbon monolith prepared by activation at 500 °C for 2 h.

### Characterization

The adsorption/desorption isotherms of active carbon monoliths were measured at 77 K using an automatic surface area and pore analyzer (SSA-4300, Beijing Builder Corp., China) after the manually-crushed monoliths with sizes of > 4 mm were degassed at 250 °C for 3 h. The apparent specific surface area ($S_{BET}$) and micropore volume ($V_{micro}$) were determined using the BET equation and t-plot method, respectively. The total pore volume ($V_t$) was estimated to be the liquid volume of $N_2$ adsorbed at a relative pressure of

0.95. The mesopore volume ($V_{meso}$) was calculated by subtracting the micropore volume from the total pore volume. The micropore percentage ($V_{micro}/V_t$) was recorded as the ratio of the micropore volume to the total pore volume. The pore size distribution curves were obtained using the Barrett-Joyner-Halenda (BJH) method.

Surface morphology measurements were performed using a scanning electron microscope (S-4800, HITACHI Corp., Japan). The carbon samples were coated with gold using a gold-sputtering device for clear visibility of the surface morphology.

The ACM bulk density was recorded as its mass/volume ratio. The volume was calculated from the height and the top-surface diameter of the ACM, including the total pore volume. The reported bulk density is the average of two replicates.

The yield for ACM was recorded as the dry-basis weight ratio of the ACM to its precursor (aspen sawdust). The weight was determined using an analytical balance (SQP, Satorius, Germany) with a sensitivity up to 0.0001 g.

X-ray diffraction (XRD) of ACMs was performed on an X-ray diffractometer (Max2500PC, MacScience Corp., Japan) using an acceleration voltage of 30 kV and a current of 100 mA. The diffraction angle was scanned from 10° to 70° $2\theta$ at 8° /min. The interplanar spacing ($d_{002}$) was calculated from $d_{002}=\lambda/2\sin\theta$, where $\lambda$ is the wavelength of the incident X-ray (0.154056 nm) and $\theta$ is the Bragg angle. The crystallite dimension parameters, including stack height ($Lc$) and stack width ($La$), were determined using the Debye-Scherrer equations: $Lc = 0.89\lambda/\beta\cos\theta$ and $La = 1.84\lambda/\beta\cos\theta$, where $\beta$ is the full width at half maximum (FWHM).

## RESULTS AND DISCUSSION

### Morphology of ACMs

Figure 1a shows photos of two active carbon monoliths (ACMs). The ACMs were visually crack-free and coin-shaped, although their preparation conditions were different.
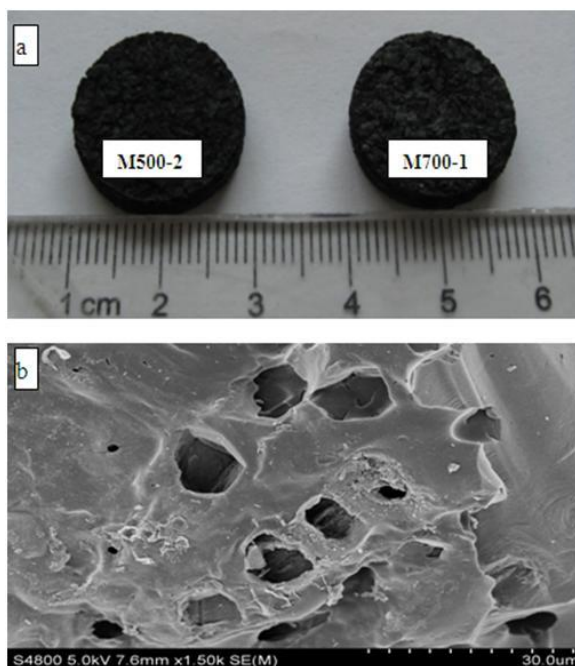


**Fig. 1.** Morphology of active carbon monoliths: (a) photos of active carbon monoliths, (b) SEM image for M700-1 at a magnification of 1500

The SEM image for M700-1 (Fig. 1b) showed that pipe-like macropores with typical sizes of 1 to 9 μm were present on the external surface.

## Yield of ACMs

The yield of ACMs (Fig. 2) was in the range of 26.6% to 36.2%, which was close to the typical yield range for $H_3PO_4$-activated carbons prepared from other types of biomass (30 to 50%) (Kennedy *et al.* 2004; Timur *et al.* 2006; Rosas *et al.* 2008). The yield decreased with increasing activation temperature or retention time, which coincided with the observations of other researchers (Kennedy *et al.* 2004; Rosas *et al.* 2008). The increment in activation temperature or retention time could promote the dehydration or gasification of the carbonaceous precursors (Kennedy *et al.* 2004; Timur *et al.* 2006; Rosas *et al.* 2008). Hence, more elements could be stripped away from the precursors, resulting in a lower yield.
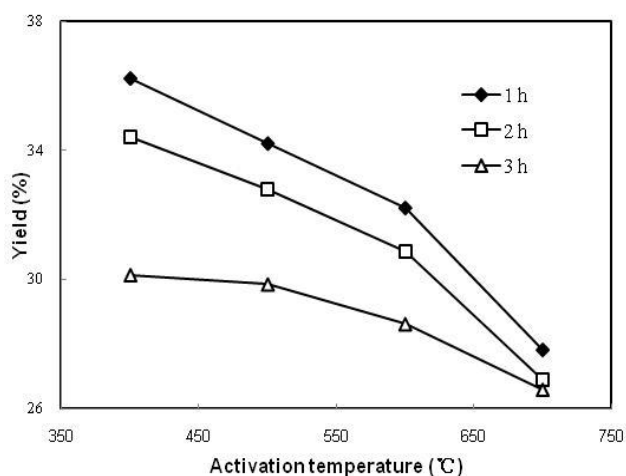


**Fig. 2.** Yield of active carbon monoliths

## XRD Analysis

The diffraction patterns of active carbon monoliths (ACMs) are shown in Fig. 3.
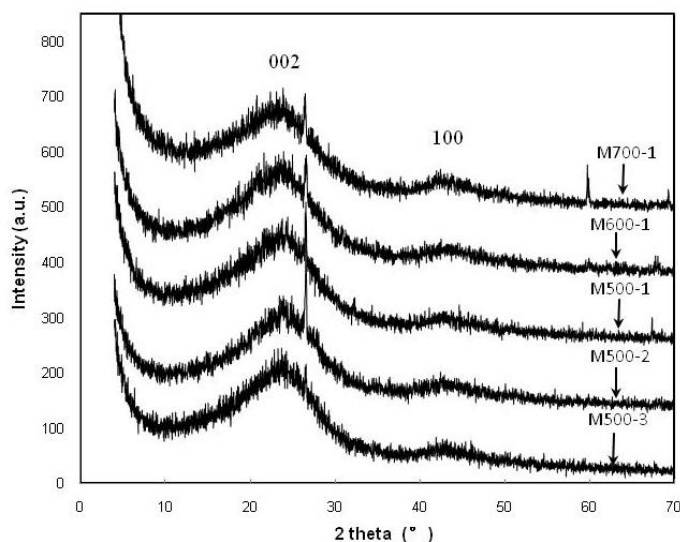


**Fig. 3.** XRD diffraction patterns of active carbon monoliths

The two broad peaks located at around 23° and 43° were reflections from the 002 and 100 planes of turbostratic carbon structures in the ACMs (Lim *et al.* 2011; Tang *et al.* 2012). These broad peaks proved the carbon structure to be amorphous (Tang *et al.* 2012). The sharp peaks at about 27 ° are due to the presence of $SiO_2$, which is commonly found in biomass (Taer *et al.* 2011).

The microcrystalline structure parameters of ACMs are presented in Table 1. The interplanar spacing ($d_{002}$) increased with increasing activation temperature or activation time, indicating that the turbostratic degree was more apparent for ACMs prepared at increased activation temperatures or retention times (Tang *et al.* 2012). The rise in activation temperatures or retention times decreased *Lc*, but hardly varied *La*, suggesting that the microcrystalline size was reduced (Tang *et al.* 2012).

**Table 1.** Microcrystalline Structure Parameters of Active Carbon Monoliths

| Sample | $d_{002}$* (nm) | $L_c$* (nm) | $L_a$* (nm) |
|--------|--------|--------|--------|
| Effects of activation temperature | | | |
| M500-1 | 0.364 | 1.46 | 3.06 |
| M600-1 | 0.369 | 1.42 | 3.05 |
| M700-1 | 0.374 | 1.01 | 3.04 |
| Effects of retention time | | | |
| M500-1 | 0.364 | 1.46 | 3.06 |
| M500-2 | 0.372 | 1.41 | 3.04 |
| M500-3 | 0.382 | 1.08 | 3.04 |

*$d_{002}$, interplanar spacing; *Lc*, stack height; *La*, stack width

## Textural Properties of ACMs

Figure 4a displays the $N_2$ adsorption-desorption isotherms of $H_3PO_4$-activated carbon monoliths prepared at different activation temperatures and retention times. The adsorption-desorption isotherms for each ACM were almost horizontal over a wide range of pressures. According to IUPAC classification, these isotherms were of type I. Hence, the monoliths were microporous (Gao *et al.* 2011), showing a high micropore percentage (87.0 to 93.4%, Table 1). Similar results were observed for binderless $H_3PO_4$-activated carbon monoliths prepared from coconut shell and African palm stones (Vargas *et al.* 2011). The small hysteresis loops observed at medium relative pressures showed the existence of mesopores. These results coincided with Fig. 4b, which shows the presence of mesopores with sizes of 2 to 7 nm, and with Fig. 1b, which reveals the existence of macropores. Additionally, Fig. 4a showed that ACMs prepared at different activation temperatures and retention times exhibited different $N_2$ adsorption capacities, suggesting that the two process parameters could affect the pore structure of ACMs.

The textural properties of ACMs are presented in Table 2. The specific surface areas (SSAs) for the crushed M700-1 with sizes of >4 mm and those with sizes of <0.9 mm were found to be 946 $m^2$/g and 955 $m^2$/g, respectively. The small difference in the SSA (9 $m^2$/g) indicated that the pore structure could hardly be modified by the crushing process. Hence, the use of crushed ACMs with sizes of >4 mm for the characterization of the textural properties of ACMs was acceptable. The largest apparent specific surface area (SSA) of the ACMs was $951 \pm 10$ $m^2$/g (average of three replicates), which was on par with the SSA of ACMs prepared from olive stones (532 to 1014 $m^2$/g) (Djeridi *et al.* 2013), rubber wood sawdust (534 to 913 $m^2$/g) (Taer *et al.* 2011), and *Pinus sylvestris*

(483 to 1152 m$^2$/g) (Laszlo *et al.* 2005). The large SSA indicated that the ACM was highly porous and potentially applicable in gas adsorption and wastewater treatment. With increasing activation temperature, the SSA, pore volume, and micropore volume increased monotonously, while the mesopore volume varied only slightly, suggesting that the increased activation temperature led to the formation of new micropores. The formation of new micropores may be attributable to the release of volatile components caused by pyrolysis (Kennedy *et al.* 2004; Guo and Rockstraw 2007). At higher temperatures, more volatile components were released, as shown by the reduction in yield. Hence, more micropores were created. Another probable explanation for the formation of the micropores was that increasing activation temperature led to incorporation of more phosphorus into the carbonaceous precursors in the form of phosphates or polyphosphates (Rosas *et al.* 2008). After they were removed from the precursors, more micropores were created. An increase in the SSA and pore volume with increasing activation temperature was also found for H$_3$PO$_4$-activated carbon prepared from corncob (Kennedy *et al.* 2004) and olive stones (Djeridi *et al.* 2013).
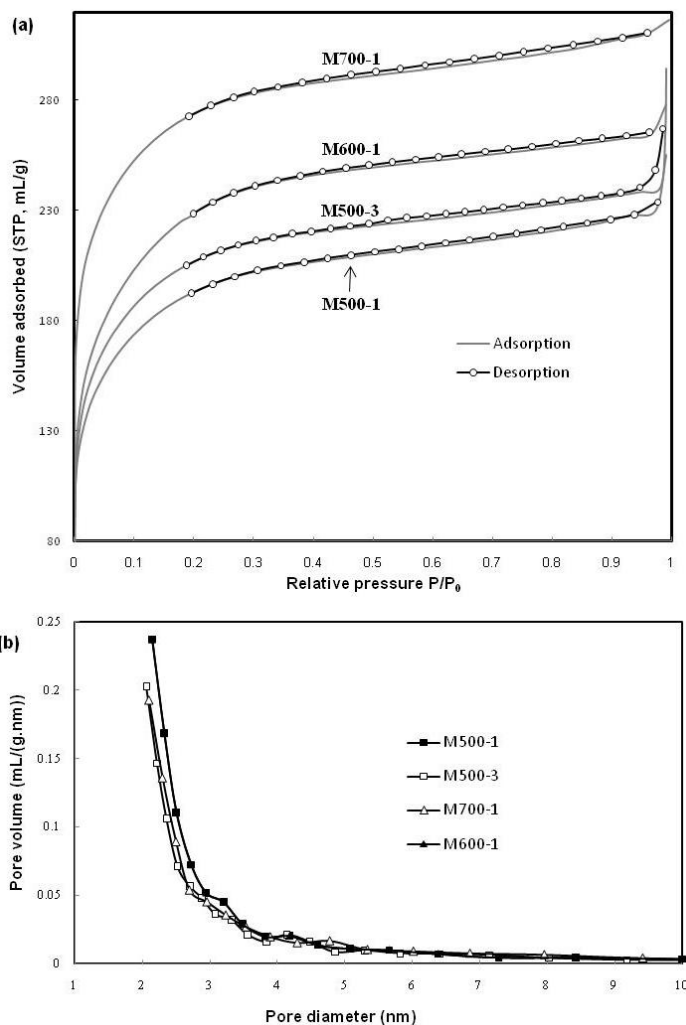


**Fig. 4.** (a) Adsorption/desorption isotherms and (b) pore size distributions of active carbon monoliths

An increase in retention time from 1 to 2 h increased the SSA, pore volume, and micropore volume, but decreased the mesopore volume, indicating that the increased retention time led to the creation of micropores and contraction of mesopores. As the retention time increased, more volatile components were released by pyrolysis, and/or more phosphorus-containing species incorporated into the precursors might be removed by washing. Hence, new micropores were created, with a concomitant deformation of mesopores, which might explain the contraction of the mesopores. However, when the retention time was further prolonged, the SSA, pore volume, and micropore volume diminished, while the mesopore volume rose. This observation suggested that the further increase in retention time resulted in pore widening of micropores into mesopores or macropores. This widening was attributable to the deterioration of the wall between adjacent pores or to the external ablation of the carbon particles (Taer *et al.* 2011). The observation that the increase in retention time first increased the SSA and pore volume, and then decreased them, was also found for the production of porous carbon from rubber wood sawdust (Taer *et al.* 2011) and waste *Ramulus mori* (Tsang *et al.* 2007).

The bulk density was found to decrease with increasing activation temperature, but only varied slightly with increasing retention time (Table 2). At higher activation temperatures, the weight loss was greater, as demonstrated by the decrease in yield. Hence, the bulk density was reduced. However, with the rise in retention times, the rate of weight loss was close to that of dimensional shrinkage (Taer *et al.* 2011), hence rendering the bulk density almost constant.

**Table 2.** Textural Properties of $H_3PO_4$-activated Carbon Monoliths Prepared at Different Activation Temperatures and Retention Times

| Samples | $S_{BET}$ (m$^2$/g) | $V_t$ (mL/g) | $V_{micro}$ (mL/g) | $V_{meso}$ (mL/g) | $V_{micro}/ V_t$ (%) | Bulk Density (g/mL) |
|---|---|---|---|---|---|---|
| | | | Effect of activation temperature | | | |
| M700-1 | 951 | 0.481 | 0.438 | 0.043 | 91.1 | 0.56±0.01 |
| M600-1 | 817 | 0.409 | 0.368 | 0.041 | 90.0 | 0.62±0.01 |
| M500-1 | 688 | 0.355 | 0.309 | 0.046 | 87.0 | 0.69±0.01 |
| | | | Effect of retention time | | | |
| M500-1 | 688 | 0.355 | 0.309 | 0.046 | 87.0 | 0.69±0.01 |
| M500-2 | 816 | 0.409 | 0.385 | 0.024 | 93.4 | 0.70±0.01 |
| M500-3 | 733 | 0.371 | 0.337 | 0.034 | 90.8 | 0.69±0.01 |

## CONCLUSIONS

1. Waste aspen sawdust can be used as a raw material for the preparation of binderless active carbon monoliths (ACMs) with high porosities.

2. Highly microporous ACMs with a micropore percentage of 91.1%, an apparent specific surface area of 951 m$^2$/g, a pore volume of 0.481 mL/g, a bulk density of 0.56 g/mL, and a yield of 27.8% could be produced by activation with $H_3PO_4$ at 700 °C for 1 h.

3. Increasing the activation temperature or retention time increased the porosity and the turbostratic degree, but decreased the yield.

## ACKNOWLEDGEMENTS

## REFERENCES CITED

Djeridi, W., Ouederni, A., Wiersum, A. D., Llewellyn, P. L., and El Mir, L. (2013). "High pressure methane adsorption on microporous carbon monoliths prepared by olives-stones," *Mater. Lett.* 99(5), 184-187.

Gao, P., Liu, Z. H., Xue, G., Han, B., and Zhou, M. H. (2011). "Preparation and characterization of activated carbon produced from rice straw by $(NH_4)_2HPO_4$ activation," *Bioresource Technol.* 102(3), 3645-3648.

Guo, Y., and Rockstraw, D. A. (2007). "Activated carbons prepared from rice hull by one-step phosphoric acid activation," *Micropor. Mesopor. Mat.* 100(1-3), 12-19.

Kennedy, L. J., Vijaya, J. J., and Sekaran, G. (2004). "Effect of two-stage process on the preparation and characterization of porous carbon composite from rice husk by phosphoric acid activation," *Ind. Eng. Chem. Res.* 43(8), 1832-1838.

Laszlo, K., Onyestyak, G., Rochas, C., and Geissler, E. (2005). "Honeycomb carbon monoliths from *Pinus sylvestris*," *Carbon* 43(11), 2402-2405.

Lim, H. N., Kassim, A., Lim, S. P., Nizar, N. S. R., and Huang, N. M. (2011). "Microstructural changes of carbonaceous monoliths synthesized via hydrothermal method," *J. Chil. Chem. Soc.* 56(1), 584-586.

Liu, L., Liu, Z., Yang, J., Huang, Z., and Liu, Z. (2007). "Effect of preparation conditions on the properties of a coal-derived activated carbon honeycomb monolith," *Carbon* 45(14), 2836-2842.

Nakagawa, Y., Molina-Sabio, M., and Rodriguez-Reinoso, F. (2007). "Modification of the porous structure along the preparation of activated carbon monoliths with $H_3PO_4$ and $ZnCl_2$," *Micropor. Mesopor. Mat*. 103(1-3), 29-34.

Rosas, J. M., Bedia, J., Rodriguez-Mirasol, J., and Cordero, T. (2008). "Preparation of hemp-derived activated carbon monoliths: Adsorption of water vapor," *Ind. Eng. Chem. Res.* 47(4), 1288-1296.

Si, C.L., Wu, L., and Zhu, Z.Y. (2009). "Phenolic glycosides from *Populus davidiana* bark," *Biochem. Syst. Ecol*. 37(3), 221-224.

Taer, E., Deraman, M., Talib, I. A., Awitdrus, A., Hashmi, S. A., and Umar, A. A. (2011). "Preparation of a highly porous binderless activated carbon monolith from rubber wood sawdust by a multi-step activation process for application in supercapacitors," *Int. J. Electrochem. Sci.* 6(8), 3301-3315.

Tang, Y. B., Liu, Q., and Chen, F. Y. (2012). "Preparation and characterization of activated carbon from waste *Ramulus mori*," *Chem. Eng. J.* 203, 19-24.

Timur, S., Kantarli, I. C., Ikizoglu, E., and Yanik, J. (2006). "Preparation of activated carbons from Oreganum stalks by chemical activation," *Energ. Fuels* 20(6), 2636-2641.

**bioresources.com**

Tsang, D. C. W., Hu, J., Liu, M. Y., Zhang, W. H., Lai, K. C. K., and Lo, I. M. C. (2007). "Activated carbon produced from waste wood pallets: Adsorption of three classes of dyes," *Water Air Soil Poll.* 184(1-4), 141-155.

Vargas, D. P., Giraldo, L., and Moreno-Pirajan, J. C. (2009). "Adsorption and structural characterization by adsorption and X-ray diffraction of activated carbon monoliths from coconut shell and African palm cuesco," *Afinidad* 66(544), 493-497.

Vargas, D. P., Giraldo, L., and Moreno-Pirajan, J. C. (2010). "Preparation and characterization of activated carbon monoliths with potential application as phenol adsorbents," *E-journal of Chemistry* 7(2), 531-539.

Vargas, D. P., Giraldo, L., Silvestre-Albero, J., and Moreno-Pirajan, J. C. (2011). "$CO_2$ adsorption on binderless activated carbon monoliths," *Adsorption* 17(3), 497-504.

Vargas, D. P., Giraldo, L., and Moreno-Pirajan, J. C. (2012). "$CO_2$ adsorption on activated carbon honeycomb-monoliths: A comparison of Langmuir and Toth models," *Int. J. Mol. Sci.* 13(7), 8388-8397.